Abundance index of Taiwanese PBF fisheries based on traditional and spatiotemporal delta-generalized linear mixed models

Shui-Kai Chang[1], Tzu-Lun Yuan[1], Hung-I Liu[2] and Haikun Xu[3]

[1]*National Sun Yat-sen University, Kaohsiung, Taiwan*
[2]*Overseas Fisheries Development Council, ROC, Taipei, Taiwan*
[3]*Inter-American Tropical Tuna Commission, La Jolla, CA, USA*

March 2020

Working document submitted to the ISC Pacific bluefin tuna Working Group, International Scientific Committee for Tuna and Tuna-Like Species in the North Pacific Ocean (ISC), from 2 to 12 March 2020, Shimizu, Japan.
Document should not to be cited without author's permission.

Summary

PBF was an important seasonal target species to Taiwan offshore longline fishery, but only market landing data with small coverage of logbooks were available before 2010. Several alternative procedures were thus used to reconstruct catch and effort data for the fishery starting from 2001, taking advantage of voyage data recorder (VDR) data, trip data and CDS data. Previously, the CPUE series from the reconstructed data were standardized using traditional delta-generalized linear mix model (delta-GLMM), and only the relative series from the southern fishing ground was adopted for stock assessment considering its features of better data stability and much higher proportion of historical catches than the northern series. This work provides the results of applying vector-auto-regressive spatiotemporal model (VAST) to the catch and effort data (with shorter time period due to the availability of geolocation information) to derive the abundance indices for the southern, northern and combined fishing grounds. As suggested by the 2nd PBFWG in 2019, four models were conducted and reported in this study, while the index of the southern fishing ground of non-spatial standardization model without data of the first two years (2001 and 2002) were considered most representative for this fleet.

Introduction

Pacific bluefin tuna (PBF) was seasonally targeted by Taiwanese offshore (small-scale) longline fishery during May to July. The longline catch had been as high as 3,089 mt in 1999 but continuously declined to the lowest record of 210 mt in 2012. Thereafter, the catch slowly bounced back and stayed at the level of 400–550 mt during 2014–2017, reaching the peak of 552 mt in 2015. The 2018 catch was 369 mt, smaller than 416 mt of 2017 due to the decrease of number of vessels applied for fishing PBF. The 2019 catch was preliminarily estimated to be higher than previous three years as 491 mt, with more vessels participated in the harvest.

PBF was traditionally caught in the southeastern waters off Taiwan (the southern fishing ground, Fig. 1); less than 10% of annual catch was from the northeastern waters off Taiwan (the northern fishing ground, Fig. 1) before 2008. The percentage of annual catch from the northern fishing ground was gradually increased to 18%–26% during 2008–2012 and then jumped to 54% in 2015 and stayed at the level of 30–46% thereafter.

Average size of PBF caught by the Taiwanese longline fishery was around 212–220 cm before 2008 (Fig. 2). Thereafter, the average in northern fishing ground stably stayed at 218–227 cm during 2008–2019; while in southern fishing ground the average gradually increased since 2008, to 234 cm in 2012, and declined all the way to 218 and 211 cm in 2018 and 2019, respectively, showing a different trend from the northern ground. The substantial increase of average size in the southern ground was considered resulting from the decline of recruitment to the fishing ground; and the decrease since 2013 was a response to more smaller fish recruited to the fishing ground and more large fish removed from the fishing ground (Fig. 3).

The PBF logbook information for Taiwanese offshore longline fishery was considered incomplete and insufficient to conduct CPUE analyses. To enhance the management on PBF fishery, Taiwan implemented specific regulations (catch documentation scheme, CDS) on the fishery since 2010. Thereafter many information on PBF fishery was available for retrospectively constructing the catch and effort data for the years before 2010. Documents ISC/15/PBFWG-2/10, ISC/16/PBFWG-1/02(revised) and ISC/17/PBFWG-1/02 (Chang et al., 2015; Chang and Liu, 2016, 2017) explained the procedures to rebuild the historical data, and the procedures were later published in Chang et al. (2017). All these works standardized the CPUE separately for the southern and the northern fishing grounds since the two fishing grounds exhibited different sizes of fish and continuity of catch series, and the CPUE index for the southern fishing ground (the traditional one) was recommended to be used for the PBF stock assessment since 2016 PBFWG meetings based on statistical performance.

The abovementioned works (non-spatial standardization) did not consider spatial effect in the model until the work of ISC/19/PFBWG-1/02 (Liu and Chang, 2019) which included a geostatistical component in the delta-generalized linear mix model (GLMM). It applied the geostatistical ordinary kriging method (Bailey and Gatrell, 1995) to interpolate minimum error-variance estimate of unsampled CPUE from the observed CPUEs based on the distance between points, and the geostatistical residuals of the observed CPUE and interpolated CPUE were used as a covariate in the GLMM. The result of this geostatistical model, however, did not improve much than the non-geo-model based on comparisons of bootstrap-R^2 (see Chang et al., 2017, 2019 for the calculation of bootstrap-R^2).

In order to address the research priority identified in the 2018 PBFWG (ISC, 2018, Attachment 4) that to “improve Taiwanese index with focus on spatiotemporal change”, another trial was made in ISC/19/PBFWG-2/11 (Yuan et al., 2019) to standardize the CPUE using vector-auto-regressive spatiotemporal model (VAST; Thorson and Barnett, 2017) that fitted to the same dataset as in ISC/19/PBFWG-1/02 but with smaller area and shorter time period that will be explained in the section of Material and Method. Based on the discussion and comments from the 2nd PBFWG in 2019 (data preparation meeting), this study performed four standardization runs including using both traditional GLMM and spatiotemporal VAST with updated data of 2019. The four runs were: standardizing the catch and effort data of whole dataset using delta-GLMM (same as the non-geo-model in 1st PBFWG in 2019) for the period of 2001-2019 (GLMM-1) and 2003-2019 (GLMM-2); and, standardizing the data of core area using VAST for the period of 2007-2019 for southern and northern fishing grounds separately (VAST-1) and for two-region combined (VAST-2).

Materials and Methods

<u>Data</u>

The catch and effort data (number of fish and fishing days) used in this study is similar to those used in ISC/19/PBFWG-2/11 (Yuan et al., 2019). Some remarks on the data are provided in the followings. First, 2018 data was slightly updated and new 2019 data was added.

Second, the whole series data is from 2001 to 2019, but as indicated in the data preparation meeting (2nd PBFWG meeting in 2019), the first two years data (2001 and 2002) have the lowest data representativeness for the whole period in terms of the proportion of the catches in the catch/effort data for analyses to the annual total catch (20~40%). Also, the quality of the trip information to construct the effort data (fishing days) for the two years was concerned. Therefore, this study tested two series of data for non-spatial standardization: whole series of data (2001-2019) and removing the first two years data (2003-2019).

Third, detailed spatial information that is important for the spatiotemporal standardization was available only since 2007; data before that year contains only the information that assigns the trip to the northern or southern fishing ground (as defined in Fig. 1) based on the starting fishing port of the trip (Chang et al., 2017). Therefore, only 2007-2019 data is used for spatiotemporal VAST analyses.

Four, PBF were caught in a wide range of northwestern Pacific Ocean, however, most PBF was caught in the waters off eastern Taiwan. To avoid the effect from the sparse spatial data away from eastern Taiwan, the data used for spatiotemporal study was narrowed down to the core-area of eastern Taiwan: 120–126ºE, 18–28ºN. The core-area data has removed only 6.8% of PBF catch from the original data for the whole period of 2007–2019.

Non-spatial model

The design of traditional non-spatial model is identical to the one used in ISC/19/PBFWG-1/02: standardizing the catch and effort data using delta-generalized linear mix model (delta-GLMM) which separately estimates the proportion of positive PBF catches assuming a binomial error distribution (zero-proportion model), and the mean catch rate of positive catches by assuming a lognormal error distribution (positive-catch model). The standardized index is the product of these two estimated components. Akaike and Bayesian information criteria was used to determine the most favorable variable composition of standardization models.

Covariates considered in the GLMM included: year (2001–2019 or 2003–2019), month (May–July), fishing area (northern and southern fishing ground separated by 24.3°N), and vessel size (CT1–CT4). Since the number of explanatory variables considered in the study was small (due to limitation in available information), simpler backward (decreasing variables) and forward (increasing variables) methods were applied when determining the variables to be included in the model (α=0.05). All the explanatory variables were included initially in the model and were determined in the final models through backward method. First order interactions of the explanatory variables were also considered for the model and were determined through forward method. The interaction of year and month was treated as random variable, while the others were treated as fix variables. Three standardization runs were performed: (1) that on the area-combined data (fishing ground effect was treated as a covariate in the model); (2) that on the data from the southern fishing ground; and, (3) that on the data from the northern fishing ground. Coefficient of Variation (CV) series were calculated through balanced bootstrap approach (Gleason, 1988) for 1,000 times.

Spatiotemporal model

The R package VAST (Thorson and Barnett, 2017; Xu et al., 2019) was applied to the abovementioned data for PBF. VAST is a delta-generalized linear mixed model that separately estimates the proportion of positive PBF catches and the mean catch rate of positive catches. In this study, we model the encounter probability (*p*) for observation *i* using a logit-linked linear predictor

$$\text{logit}(p_i) = \beta_1(t_i) + L_{\omega_1}\omega_1(s_i) + L_{\varepsilon_1}\varepsilon_1(s_i, t_i) + L_{\delta_1}\delta_1(v_i)$$

and model the positive catch rate (λ) for observation i using a log-linked linear predictor:

$$\log(\lambda_i) = \beta_2(t_i) + L_{\omega_2}\omega_2(s_i) + L_2\varepsilon_2(s_i, t_i) + L_{\delta_2}\delta_2(v_i)$$

where $\beta(t_i)$ is the intercept for in year t_i, $\omega(s_i)$ denotes time-invariant spatial variations at location s_i, $\varepsilon(s_i, t_i)$ denotes time-varying spatiotemporal variations at location s_i in year t_i , and $\delta(v_i)$ denotes the effect of vessel v_i on catchability and $\delta_i(v_i) \sim \text{Normal}(0,1), i = 1,2$. L_ω, L_ε and L_δ are the scaling coefficients of the random effect distributions.

Both the spatial and spatiotemporal random effects are assumed to be correlated in space. We assume that the spatial random effect is $\omega_i \sim \text{MVN}(0, R_i), i = 1,2$ and the spatiotemporal random effect in year t is $\varepsilon_i(s,t) \sim \text{MVN}(0, R_i), i = 1,2$, where R_1 and R_2 are the correlation matrices approximating the similarity of encounter probability and positive catch rate among observation locations. The correlation between both the spatial and the spatiotemporal residuals at two locations (s and s') is assumed to decline over distance at a rate specified by the Matérn function: $R_i\ (s, s') = \kappa_i|\text{H}(s - s')|, i = 1,2$, where κ is the decorrelation scaling parameter, which controls the rate of decrease in spatial correlation with increasing distance, and H is a 2 by 2 transformation matrix describing geometric anisotropy (correlation decrease with increasing distance faster in some directions than in the others). Thus, $\kappa_i|\text{H}(s - s')|$is the standardized distance between location s and s' after accounting for geometric anisotropy (Thorson et al., 2015).

The observed catch rate (c_i) for each observation is C_i/E_i, Where C and E represent observed catch and effort, respectively. The probability function for c_i is

$$\Pr(c_i = c) = \begin{cases} 1 - p_i & \text{if } c = 0 \\ p_i \times \text{Lognormal}(c_i | \log(\lambda_i), \sigma^2) & \text{if } c > 0 \end{cases}$$

where σ^2 is a dispersion parameter.

The index of abundance of Pacific bluefin tuna (in year t) is then predicted using an area-weighted approach:

$$I_{std}(t) = \sum_{k=1}^{n_k}(a(k) \times d(k,t))$$

where n_k denotes the number of knots, $a(k)$ is the area associated with knot k, and $d(k,t)$ is the predicted density for knot k and year t:

$$d(k,t) = \text{logit}^{-1}(\beta_1(t_i) + L_{\omega_1}\omega_1(s_i) + L_{\varepsilon_1}\varepsilon_1(s_i,t_i)) \\ \times \exp\left(\beta_2(t_i) + L_{\omega_2}\omega_2(s_i) + L_2\varepsilon_2(s_i,t_i)\right)$$

Essentially, the area-weighted approach computes total abundance as the weighted sum of estimated density across the pre-defined spatial domain of knots, with weights equal to the area associated with each knot.

The fishing activities analyzed in this study took place in more than 5000 unique 0.1° x 0.1° grid cells. For computational purposes, we use the k-means algorithm to cluster all the grid cells into 50 spatial knots and assume that both the spatial and spatiotemporal random effects for a grid cell are from the closest knot in space.

Results and Discussions

Non-spatial model runs

GLMM-1 and GLMM-2 applied the same procedures of the non-spatial standardization model of ISC/19/PBFWG-1/02 on whole area data for 2001–2019 and 2003–2019, respectively. Both models fit the data well (based on the qq-plots and the residual histograms, Fig. 4) for the sub-models on southern, northern and whole fishing grounds. From AIC analyses, standardization separately by fishing grounds has better performance than the one combined both fishing grounds (Table 1); while from BIC analyses, standardization separately by fishing grounds did not show substantially smaller BIC than the one combined both grounds for GLMM-2. Even with this exception, area-separate models were considered more preferable because the size composition of the two fishing grounds apparently different. The index of the southern fishing ground was considered relatively better representing the PBF abundance index than the northern one considering its features of better data stability and with much higher proportion of historical catches.

The resulted indices are shown in Fig. 5. The new indices of GLMM-1 (for 2001–2019, lines 202003_S, 202003_N, 202003_A) are almost identical to those of ISC/19/PBFWG-1/02 (201903_S, 201903_N, 201903_A) for the overlapped period. Results of GLMM-2 (for 2003–2019) have similar to the GLMM-1.

Spatiotemporal model

Two major fishing grounds are noted from the distribution of fishing effort in the core area (fishing days, Fig. 3): southeast Taiwan and northeast Taiwan. All the spatiotemporal models (VAST-1 for southern fishing ground and for northern fishing ground separately, and VAST-2 for the combined fishing ground) have successfully converged, which were confirmed by the fact that the Hessian matrix was positive definite, and the maximum gradient component was smaller than 0.001. Moreover, quantile diagnostics suggested the spatiotemporal model fitted the catch and effort data well (Fig. 7).

Pronounced spatiotemporal variations in density were predicted for the period of 2007–2019 (Fig. 8). Predicted densities decreased from the starting year of the study (2007) to the lowest level in 2011 and 2012, and then started to increase gradually to the end year of the study (2019).

Both encounter probability and positive catch rate are more coherent along directions of northwest-southeast for VAST-1 southern ground, northeast-southwest for VAST-1 northern ground, and slightly northeast-southwest for VAST-2 (Fig. 9). The center of biomass of PBF in the east-west (left) and north-south (right) directions are computed for the model runs (Fig. 10). For the southern fishing ground, there was no clear pattern in east-west movement but has a trend of moving northward in recent years. No long-term trend was noted for the northern fishing ground. For whole core area (VAST-2), the center of biomass has been moving westward during 2013–2016 and then moving eastward, and has been generally moving northward up to 2016 and then southward thereafter.

The standardized indices computed based on the spatiotemporal distribution of predicted density showed a clear trend of sharp decline since 2007, reaching the lowest level in 2012, and then slowly and continuously recovered to the current year for VAST-1 southern fishing ground and VAST-2 whole area (Fig. 11 left panels). The effective area occupied computed from the models (Fig. 11 right panels) showed roughly similar trends with the corresponding standardized indices, but the patterns were less clear and the associated uncertainly is much larger.

The three standardized indices (for southern ground and northern ground of VAST-1, and whole area of VAST-2) were compared with those of non-spatial GLMM in Fig. 5. Indices from spatial VAST standardizations showed similar trends with those from non-spatial GLMM runs, except that spatial model results indicated substantially higher relative CPUEs in both the beginning and ending years. According to the conclusion of the data preparation meeting of the second 2019 PBFWG, the index of the southern fishing ground of GLMM-2 (removed 2001 and 2002) were considered most representative for this fleet.

References

Bailey, T.C., A.C. Gatrell. 1995. Ordinary Kriging. *In*: Interactive spatial data analysis. Chap.5.5. Longman Scientific & Technical, New York.

Chang, S.-K., H.-I Liu. and Y.-W. Fu. 2015. Estimation of standardized CPUE series on Pacific bluefin tuna for Taiwanese longline fishery under incomplete data. Pacific Bluefin Tuna Working Group Intersessional Workshop of the ISC, Kaohsiung, Taiwan, November 18-25, 2015. ISC/15/PBFWG-2/10.

Chang, S.-K. and H.-I Liu. 2016. Update of Standardized PBF CPUE Series for Taiwanese Longline Fishery. Pacific Bluefin Tuna Working Group Intersessional Workshop of the ISC, La Jolla, USA, 29 February – 11 March 2016. ISC/16/PBFWG-1/02 (revised).

Chang, S.-K. and H.-I Liu. 2017. Standardized PBF CPUE series for Taiwanese longline fishery up to 2016. Pacific Bluefin Tuna Working Group Intersessional Workshop of the ISC, Shimizu, Japan, 15 – 20 February 2017. ISC/17/PBFWG-1/02.

Chang, S.-K., H.-I Liu, H. Fukuda and M.N. Maunder. 2017. Data reconstruction can improve abundance index estimation: An example using Taiwanese longline data for Pacific bluefin tuna. PLoS ONE 12, e0185784.

Chang, S.-K., T.-L. Yuan, S.-P. Wang, Y.-J. Chang and G. DiNardo. 2019. Deriving statistically reliable abundance index from landing data: an application to Taiwanese coastal dolphinfish fishery with multi-species feature. Transactions of the American Fisheries Society 148, 106-122.

ISC. 2018. Report of the Pacific Bluefin Tuna Working Group Intersessional Workshop. ANNEX 9 of the 18th Meeting of the International Scientific Committee for Tuna and Tuna-Like Species in the North Pacific Ocean. ISC/18/ANNEX/09.

Liu, H.-I and S.-K. Chang. 2019. CPUE standardizations of Taiwanese PBF fisheries with/without geostatistical consideration. Pacific Bluefin Tuna Working Group Intersessional Workshop of the ISC, 18-22 March, 2019, Jeju, Korea. ISC/19/PBFWG-1/02.

Thorson, J.T. and L.A.K. Barnett. 2017. Comparing estimates of abundance trends and distribution shifts using single- and multispecies models of fishes and biogenic habitat. ICES Journal of Marin Sciences 74 (5), 1311–1321.

Xu, H., C.E. Lennert-Cody, M.N. Maunder and C.V. Minte-Vera. 2019. Spatiotemporal dynamics of the dolphin-associated purse-seine fishery for yellowfin tuna (*Thunnus albacares*) in the eastern Pacific Ocean. Fisheries Research 213:121-131.

Yuan, T.L., S.K. Chang, H. Xu and H.I Liu. 2019. Standardized index of relative abundance of Taiwanese PBF fisheries based on traditional and spatiotemporal delta-generalized linear mixed models. Pacific Bluefin Tuna Working Group Intersessional Workshop of the ISC, La Jolla, USA, 18 – 23 November 2019. ISC/19/PBFWG-2/11.

Table 1. Best variable combinations of the delta-lognormal mixed models for GLMM-1 (2001-2019) and GLMM-2 (2003-2019), and the Akaike information criterion (AIC) and Bayesian information criterion (BIC). (ZPM: zero-proportion model; PCM: positive-catch model)

Model type	Final model formulation	n	AIC	BIC
A. GLMM-1				
Southern fishing ground				
ZPM:	Year+Month+Year*Month	190	442.6	446.7
PCM:	Year+Month+CT+Year*Month	8539	23884.1	23888.1
Northern fishing ground				
ZPM:	Year+Month+CT+Year*Month	142	443.3	447.1
PCM:	Year+Month+CT+Year*Month	2603	6315.0	6318.4
Combined southern and northern fishing grounds				
ZPM:	Year+Month+CT+Area+Year*Month	332	982.0	986.1
PCM:	Year+Month+Area+Year*Month	11142	30349.1	30802.9
B. GLMM-2				
Southern fishing ground				
ZPM:	Year+Month+CT	172	393.3	397.2
PCM:	Year+Month+CT+Year*Month	7629	21380.1	21761.8
Northern fishing ground				
ZPM:	Year+Month+CT+Year*Month	137	429.1	432.8
PCM:	Year+Month+CT+Year*Month	2589	6230.2	6464.5
Combined southern and northern fishing grounds				
ZPM:	Year+CT+Area	309	899.1	903.0
PCM:	Year+Month+CT+Area+Year*Month	10218	27971.3	27975.1

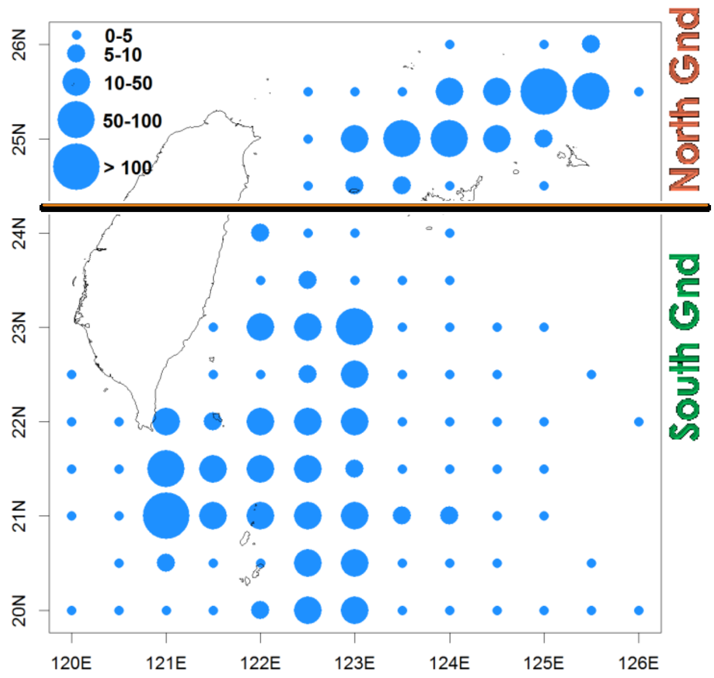

Fig. 1. Average PBF catch distribution off Taiwan for 2010–2015. The line splits the fishing grounds into southern ground and northern ground by 24.3°N.

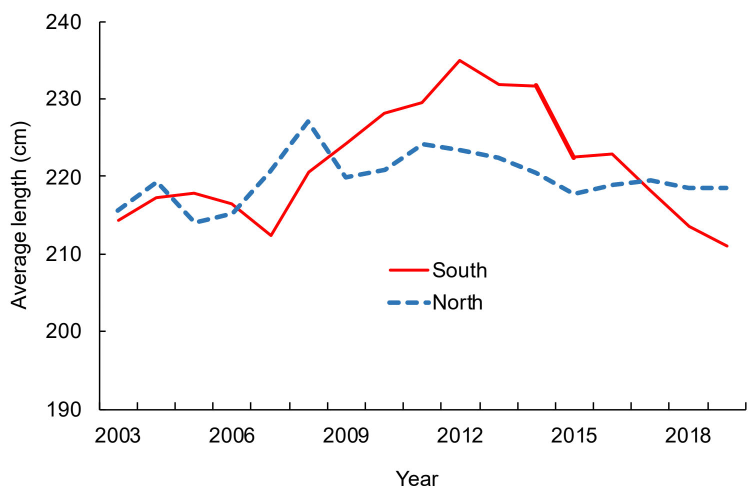

Fig. 2. Annual trend of average length of PBF of Taiwanese longline fishery, by southern and northern fishing grounds.

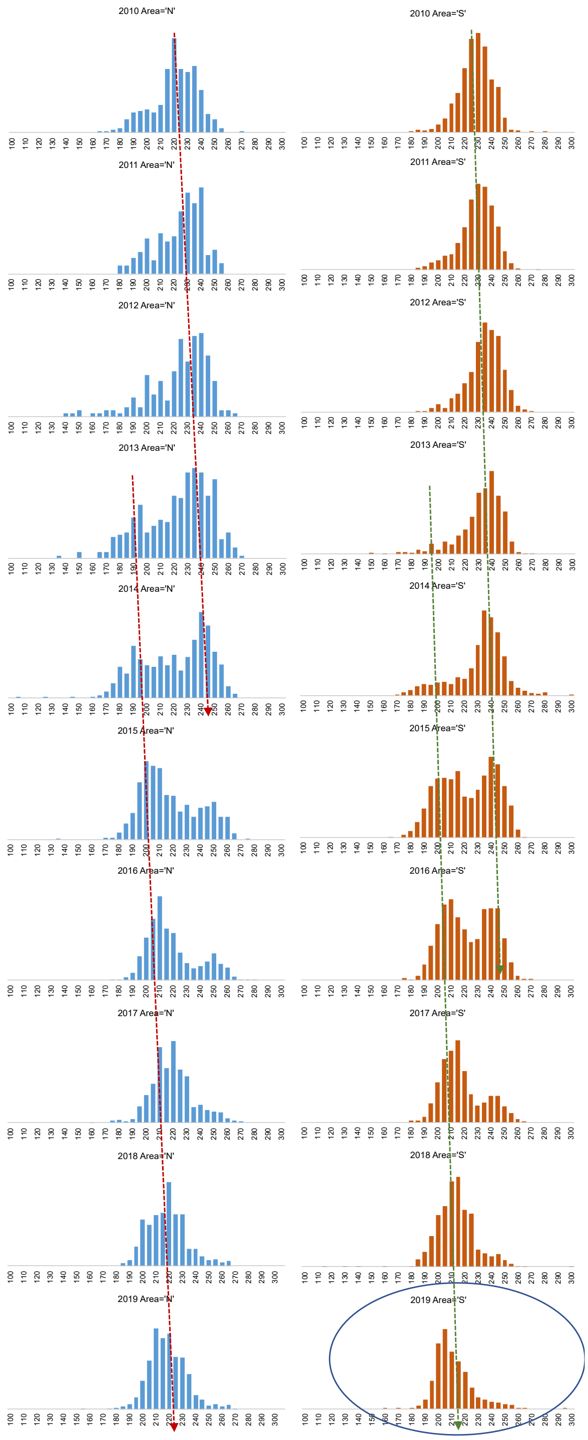

Fig. 3. Length frequencies of Taiwanese PBF during 2010 – 2019 for northern fishing ground (left in blue) and southern fishing ground (right in red).

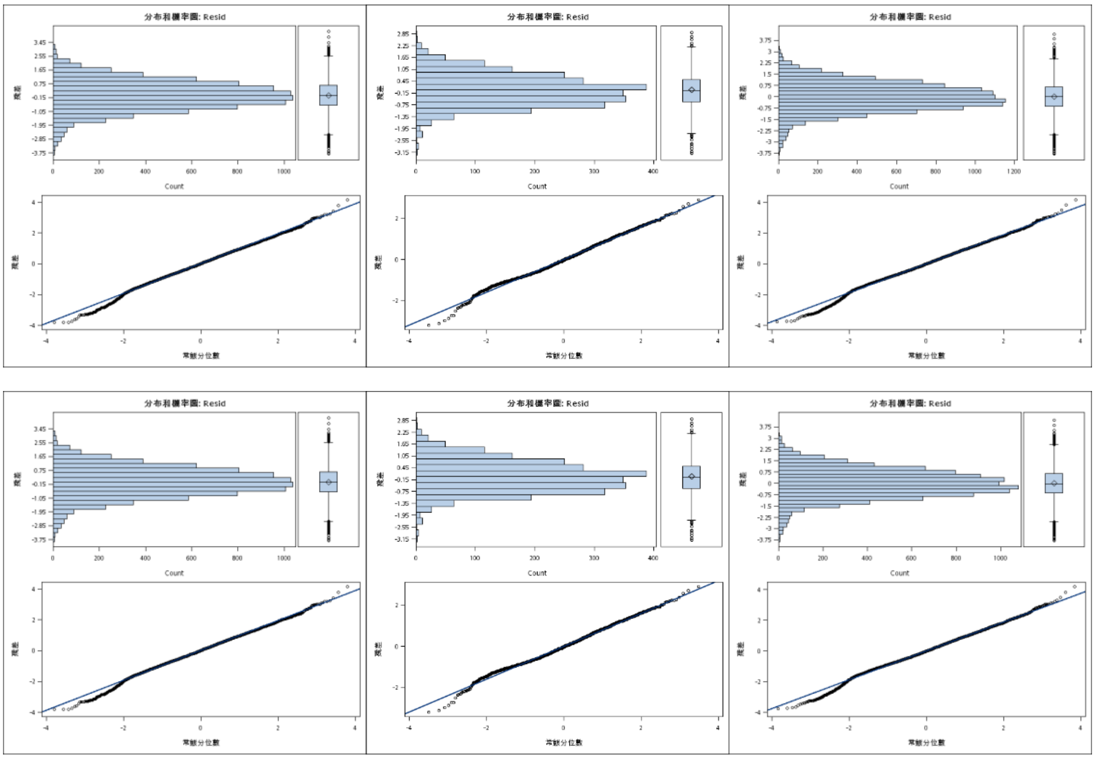

Fig. 4. Diagnostic residual plots (the posterior-predictive residual histogram and qq plot comparing the observed and predicted quantiles of CPUE given encounter) for the traditional delta-GLMM analyses. Upper panels are for years of 2001-2019 (GLMM-1) and bottom panels for 2003-2019 (GLMM-2). Panels from left to right are for the southern, northern and all fishing grounds.

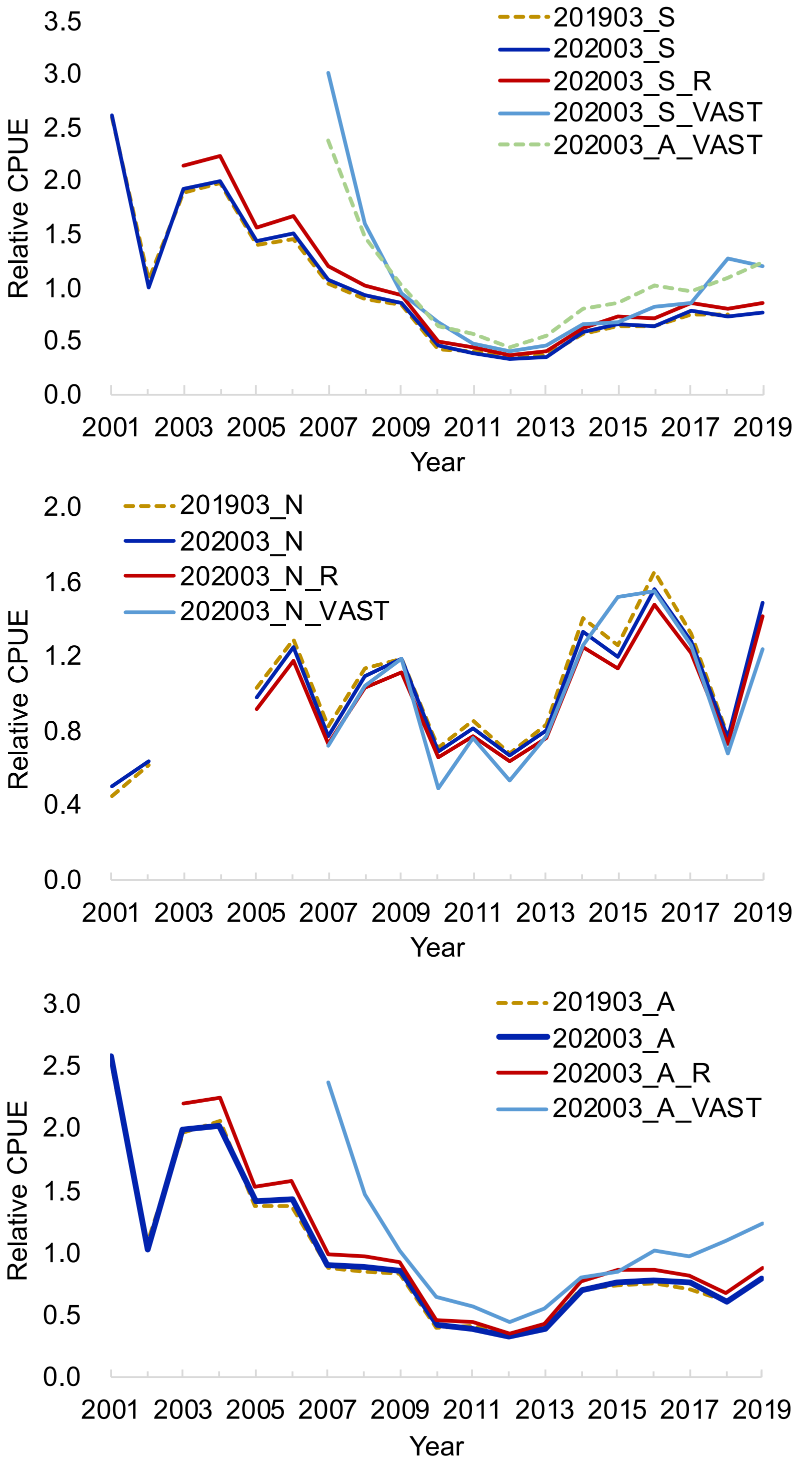

Fig. 5. Standardized abundance indexes based on traditional delta-GLMM (as in ISC/19/PBFWG-1/02) on the whole dataset and on VAST analyses on the core area data. “201903” and “202003” in the codes indicate the result for March meeting of 2019 and March meeting of 2020 (this study). Indexes based on delta-GLMM are for 2001-2019 (GLMM-1) and for 2003-2019 (GLMM-2) suffixed with “R”). “S”, “N”, and “A” in the codes indicate the results for the southern, northern, all fishing grounds (southern and northern fishing grounds combined), respectively. The lines suffixed with VAST are standardized indices based on VAST analyses.

(A) (B)

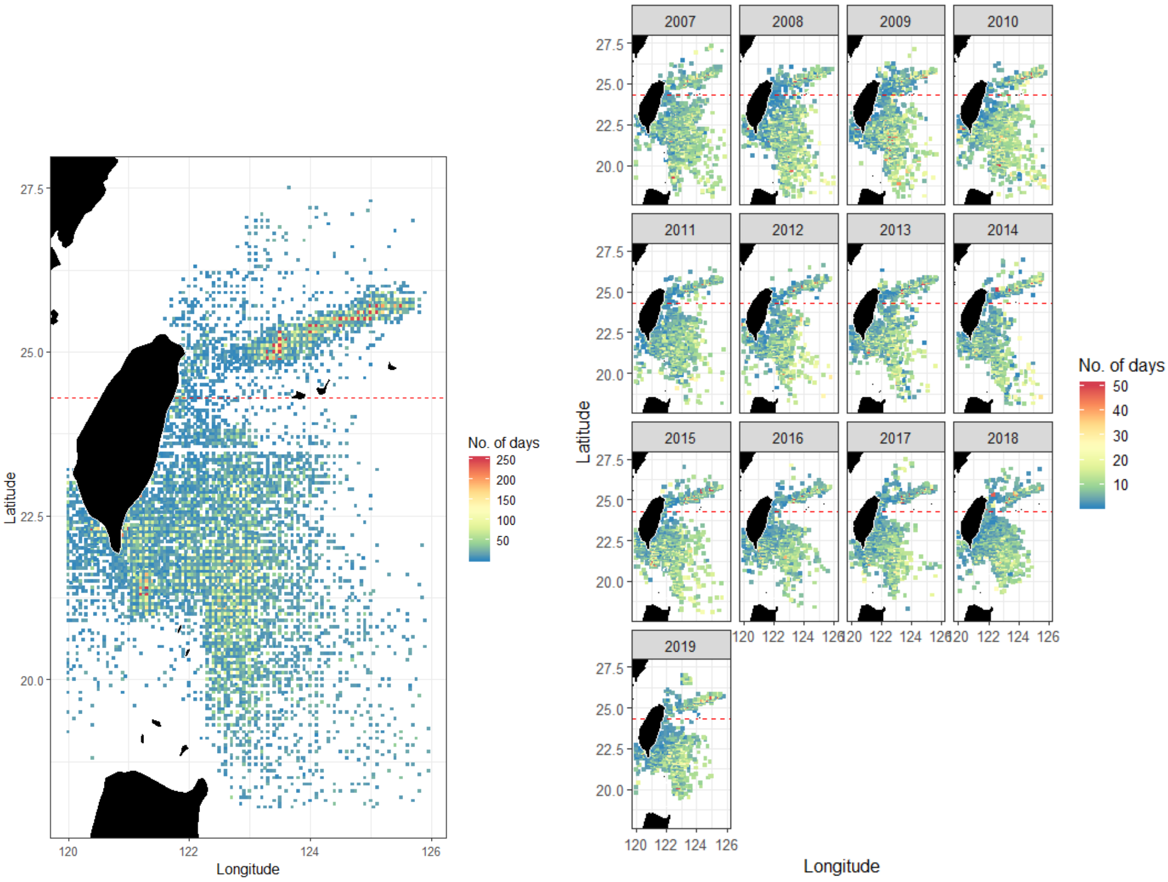

Fig. 6. Geographic distribution of fishing days per 0.1º×0.1º grid cell during 2007–2019: (A) whole period; (B) by year.

(A)

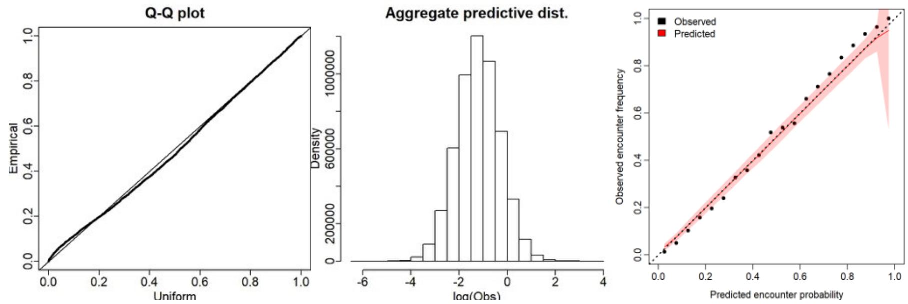

(B)

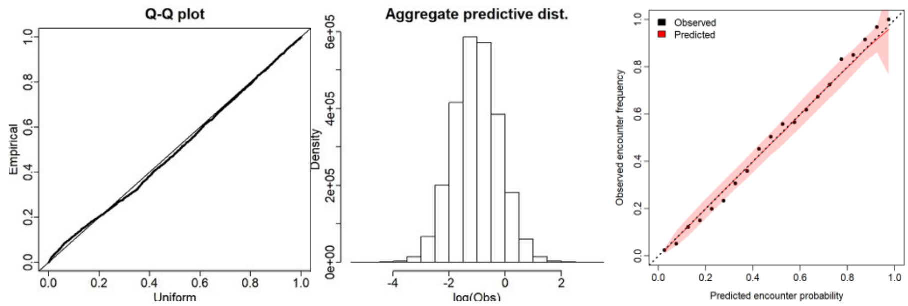

(C)

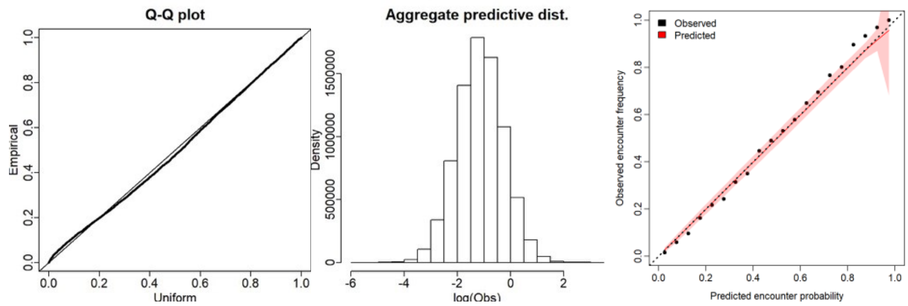

Fig. 7. Diagnostic residual plots for VAST-1 (A for Core-South fishing ground and B for Core-North fishing ground), VAST-2 (C, whole core fishing ground combined). The graphs from left to right: the qq plot comparing the observed and predicted quantiles of CPUE given encounter, the posterior-predictive residual histogram, and encounter probability.

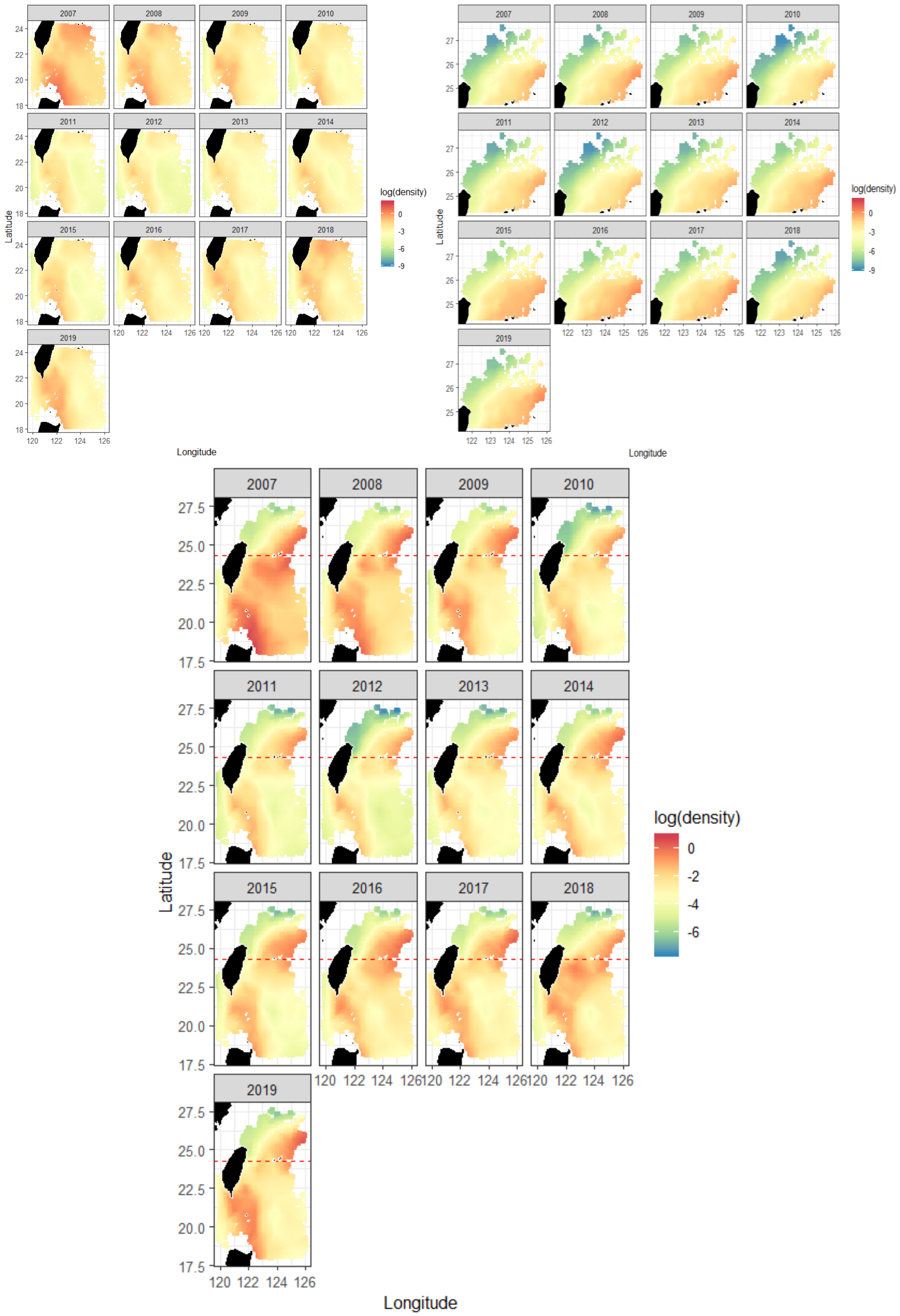

Fig. 8. Spatiotemporal distribution of predicted log density of PBF during 2007–2019 from VAST-1 (upper left – South, right – North) and VAST-2 (combined).

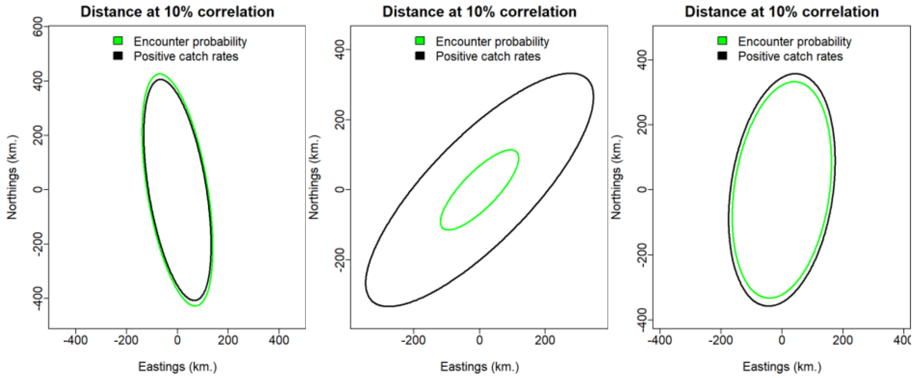

Fig. 9. Distance of 10% correlation of encounter probability and positive catch rate. From left to right: southern region of VAST-1, northern region of VAST-1 and VAST-2.

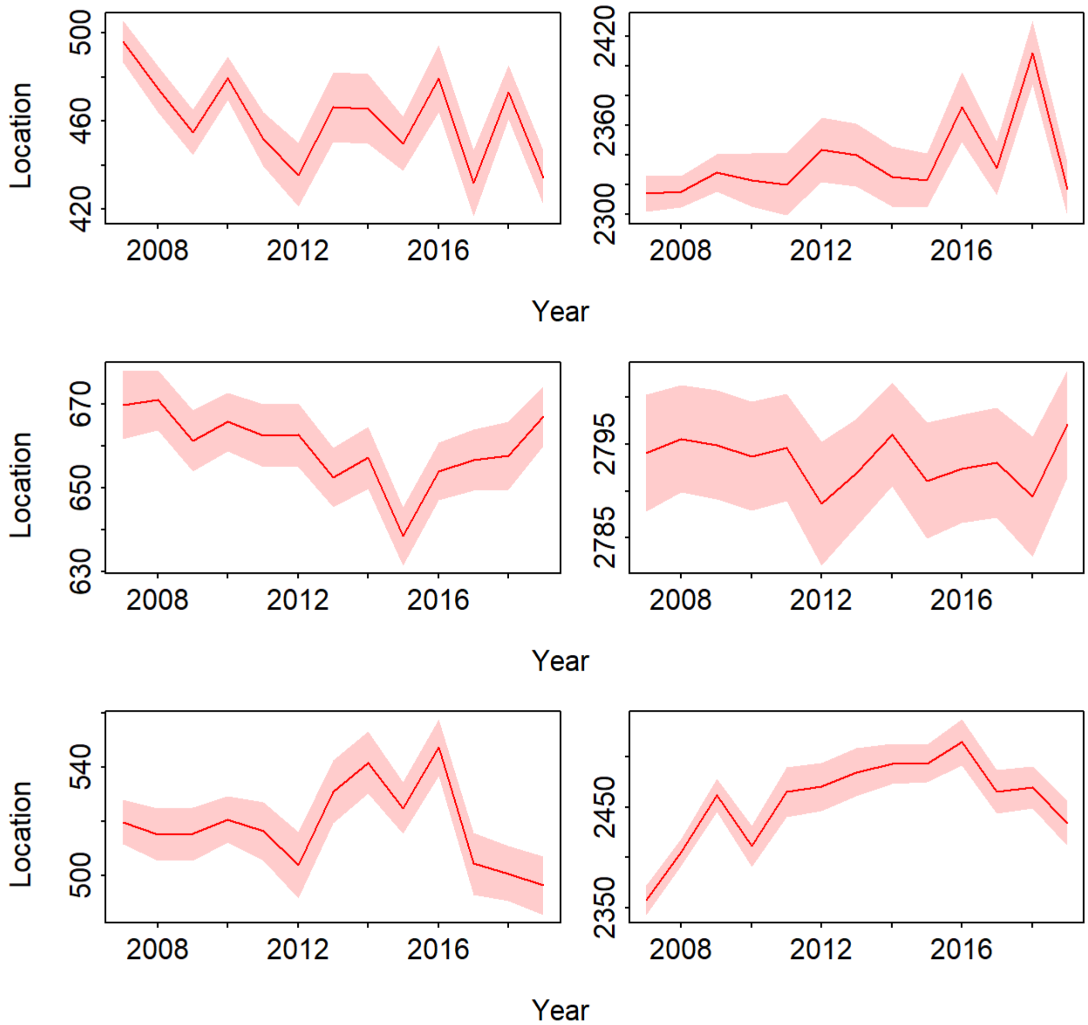

Fig. 10. The center of biomass of PBF in the east-west (left) and north-south (right) direction. From top to bottom: southern region of VAST-1, northern region of VAST-1 and VAST-2.

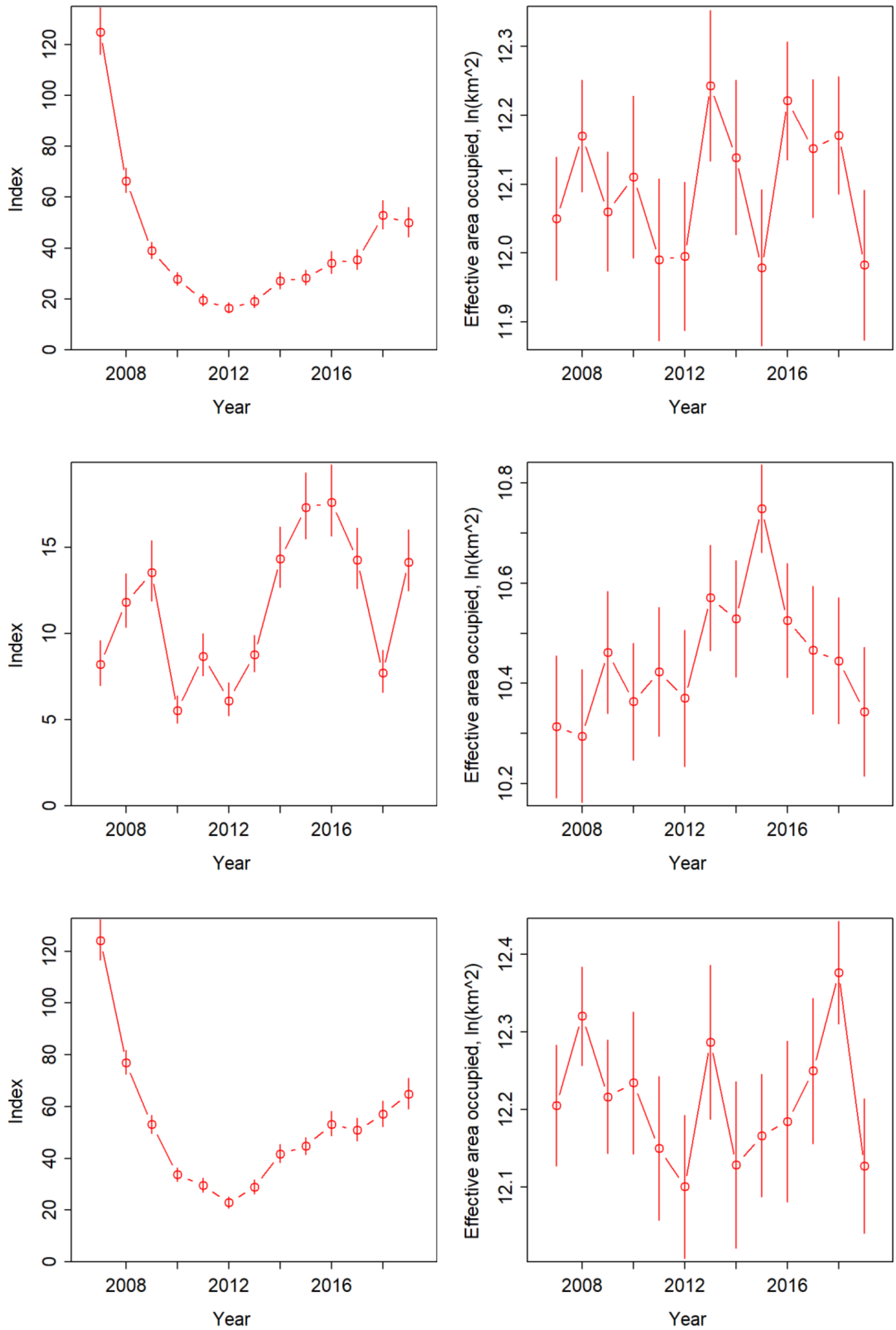

Fig. 11. Standardized index of relative abundance (left) and estimated effective area occupied (right) of PBF. The bars represent the standard errors. From top to bottom: southern region of VAST-1, northern region of VAST-1 and VAST-2.